Computer simulation study of extrinsic defects in $PbWO_4$ crystals

2003 J. Phys.: Condens. Matter 15 1963

(http://iopscience.iop.org/0953-8984/15/12/313)

INSTITUTE OF PHYSICS PUBLISHING JOURNAL OF PHYSICS: CONDENSED MATTER

J. Phys.: Condens. Matter **15** (2003) 1963–1973 PII: S0953-8984(03)56513-4

Computer simulation study of extrinsic defects in $PbWO_4$ crystals

Qisheng Lin[1] **and Xiqi Feng**

The State Key Laboratory of High-performance Ceramics and
Superfine Microstructures, Chinese Academy of Sciences, 1295 DingXi Road,
Shanghai 200050, People's Republic of China

E-mail: qslin@ameslab.gov

Received 22 November 2002, in final form 30 January 2003
Published 17 March 2003
Online at stacks.iop.org/JPhysCM/15/1963

Abstract

This paper presents the results of a simulation study of extrinsic defects in lead tungstate crystal. The results reveal that monovalent ions preferentially enter the Pb sites, whereas pentavalent ions preferentially occupy the W sites, and both of them will simultaneously produce oxygen vacancies to keep the charge neutrality. The solution energy of trivalent dopants is a strong function of the dopant's cation radius. They generally occupy the Pb sites, with the excessive charge mainly balanced by lead vacancies. In some cases, however, an oxygen interstitial ion might also coexist. Binding energy calculations demonstrate a strong tendency toward cluster formation of the trivalent dopant ions and the lead vacancies. The relationship between the aliovalent doping and the improvement of $PbWO_4$ (PWO) scintillation properties are discussed. This work enables us to comprehend the doping mechanism of PWO and has predicative value.

(Some figures in this article are in colour only in the electronic version)

1. Introduction

Recently, lead tungstate crystal, $PbWO_4$ (PWO), has attracted increasing attention because of its application as a new generation of scintillator in high-energy physics [1–3]. Up to now, much progress has been made and the project to construct an electromagnetic calorimeter (ECAL) for a compact muon solenoid (CMS) has reached its final research and development phase [4].

A good scintillator is appraised chiefly by its emission spectrum, light output, decay kinetics and radiation hardness. In the case of PWO, the light output and the radiation hardness are the two most important key factors, due to the severe environments in which it is applied [1]. These two factors are strongly affected by the colour centre absorption bands within the ultraviolet (UV) region [5–7], i.e. the absorption bands peaking around 350 and

[1] Temporary address: 344 Spedding Hall, Ames laboratory, Iowa State university, IA 50011, USA.

420 nm. How to suppress these absorption bands, therefore, has been the subject of PWO workshops all over the world.

For the nature of the problem mentioned above obviously we should look to the origins of those absorption bands. It has been well established that these absorption bands can be effectively suppressed by post-growth annealing treatments [8, 9] and aliovalent ion doping [10–14]. In methodology, the former treatment, as revealed by computer simulation [15], tries to ameliorate the scintillation properties through altering the concentration of oxygen vacancies, one of the main factors influencing the referred absorption bands [16]. On the other hand, aliovalent ion doping optimizes the crystal quality by virtue of extrinsic defects, which consist of substitutional ions foreign to the pure host lattice. The incorporation of such ions in many cases perturbs the charge balance of the crystal and therefore requires the creation of compensating defects [17], through which the intrinsic defects in the crystal are intentionally increased or decreased.

Due to the limited amount of defect chemistry knowledge on PWO, problems such as the doping mechanism and the charge compensation of defects remain unresolved. For instance, taking account of the radius and the electronegativity, most specialists [11–13] in the field of PWO consider that a trivalent ion will exclusively occupy the Pb^{2+} sites, forming a positively charged defect $(M_{Pb}^{3+})^{\cdot}$ (M denotes trivalent ions). Then it will arouse in the crystal the competition of the $(M_{Pb}^{3+})^{\cdot}$ defects and the O^{-} and/or Pb^{3+} hole centres [5, 11, 18], which leads to the above-mentioned absorption bands being suppressed. Studies of the dielectric spectrum in PWO:RE (RE $= La^{3+}, Y^{3+}$) crystals [19], however, reveal two other forms of defect: $[2(RE_{Pb}^{3+})^{\cdot}–V''_{Pb}]$ and $[2(RE_{Pb}^{3+})^{\cdot}–O''_{i}]$, indicating the existence of different charge compensation mechanisms.

Other uncertainties concern the lattice site occupied by the dopant ions, the stability of defect clusters, as well as the principles to determine which element has a positive effect and therefore should be selected. Resolving these problems is expected to improve our understanding of radiation damage mechanisms, to improve the crystal scintillation properties and to offer some useful instructions for batch crystal growth.

We have reported in another paper the simulation results on the intrinsic defects in PWO [15], where the modelling of PWO has been successfully set up and the technique has been found a powerful tool to investigate the intrinsic defects of the studied crystal. In the present paper, we continue by reporting the simulation results of the extrinsic defects in PWO. This work enables us to comprehend the defects involved in the dopant reaction and to fully understand those problems mentioned above. In this context, the results are summarized in section 3, which follows a description of the simulation method in section 2. The explanation of these results for experimental properties are discussed in section 4, followed by our conclusions.

2. Simulation methods

The lattice simulations were performed using the GULP program which is based upon the Mott–Littleton methodology [20] for accurate modelling of perfect and defect lattices. Since detailed documentation of the simulation techniques can be found elsewhere [21, 22], only a brief account will be presented here.

An important feature of these calculations is the modelling of defects. The simplification of the Mott–Littleton method is to divide the crystal lattice that surrounds the defect into three regions known as 1, 2a and 2b [20, 23, 24]. In the inner region, all interactions are treated at an atomistic level and the ions are explicitly allowed to relax in response to the defect, while the remainder of the crystal, where the defect forces are relatively weak, is treated by more approximate quasi-continuum methods. In this way, local relaxation is effectively modelled

Table 1. Short-range potential parameters.

Interactions	A (eV)	ρ (Å)	C (eV Å^6)	Reference
O^{2-}–O^{2-}	9 547.96	0.219 2	32.0	[15]
Pb^{2+}–Pb^{2+}	18 912.114	0.313 781	2.6	[15]
Pb^{2+}–O^{2-}	8 086.8038	0.264 866	3.5636	[15]
W^{6+}–O^{2-}	767.43	0.438 6	0	[15]
Li^{+}–O^{2-}	426.48	0.3	0	[30]
Na^{+}–O^{2-}	1 271.504	0.3	0	[30]
K^{+}–O^{2-}	3 587.57	0.3	0	[30]
Al^{3+}–O^{2-}	2 409.505	0.264 9	0	[30]
Fe^{3+}–O^{2-}	3 219.335	0.264 1	0	[30]
Yb^{3+}–O^{2-}	991.029	0.351 5	0	[30]
Y^{3+}–O^{2-}	1 519.279	0.329 1	0	[30]
Gd^{3+}–O^{2-}	866.339	0.377	0	[30]
Eu^{3+}–O^{2-}	847.868	0.379 1	0	[30]
Nd^{3+}–O^{2-}	13 084.217	0.255	0	[30]
La^{3+}–O^{2-}	5 436.827	0.293 9	0	[30]
Nb^{5+}–O^{2-}	1 796.3	0.345 98	0	[42]

and the crystal is not considered simply as a rigid lattice through which ion species diffuse. In this study, the inner defect region was set at 7.5 Å, which was found to be adequate for convergence of the computed energies.

Both perfect and defect lattice calculations are formulated within the framework of the Born-like model [25]. In this approximation, the potentials describing the interatomic interactions between two ions, with distance r, are presented as follows

$$U_{ij}(r) = \frac{Z_i Z_j e^2}{r} + A_{ij} \exp\left(\frac{-r}{\rho_{ij}}\right) - \frac{C_{ij}}{r^6} \tag{2.1}$$

where the first part is the long-range Coulombic term and the second the short-range term described by the two-body Buckingham form. Here, Z_i is the formal charge of atom i, and A_{ij}, ρ_{ij} and C_{ij} are the adjustable potential parameters.

Because charged defects will polarize other ions in the lattice, ionic polarizability (α) is also incorporated into the potential model. A shell model [26] treatment of such effects is described in terms of a shell with charge Y connected via an isotropic harmonic spring of force constant, k, to a massive core of charge Z–Y, namely,

$$\alpha = \frac{Y^2}{k}. \tag{2.2}$$

In the calculations, all ions are treated as polarizable: for Pb^{2+}, $Y = -0.09$, $k = 21\,006.539$ eV Å^{-2}, for W^{6+}, $Y = 5.89$, $k = 7.690$ eV Å^{-2} and for O^{2-}, $Y = -2.04$, $k = 6.300$ eV Å^{-2}.

Table 1 gives the short-range potential parameters used in this work, whereas the calculated fundamental defect energies are given in table 2.

3. Simulation results

3.1. M_2O and M_2O_5 solution

Because the concentration of dopant ions in PWO crystal is very small (about 10 ppm [1–3]), direct sensitivity to the substituted lattice sites and charge compensation can be difficult in

Table 2. Some fundamental defect energies.

Defect	Energy (eV)	Defect	Energy (eV)
V''_{Pb}	25.55	Pb^{4-}_{W}	149.99
$V^{\cdot\cdot}_{O}$	18.72	W^{4+}_{Pb}	127.55
O''_i	−9.46		

structure determination, e.g. XRD. Computer simulation, however, has been proved one of the most useful tools in this aspect [27]. Our simulation approach is based on assessing the relative energies of solutions for dopant ion substitution into the host lattice.

It has been well established that monovalent (e.g. the K^+ ion [5, 28, 29]) ion doping and pentavalent (e.g. Nb^{5+} ion [6, 12, 28]) ion doping have considerable influence on short wavelength absorption. We have considered the possible doping mechanisms of monovalent ions dissolving into the PWO lattice as follows,

$$M_2O + PWO \rightarrow 2M'_{Pb} + V^{\cdot\cdot}_{O} + 2PbO \tag{3.1}$$

$$M_2O + PWO \rightarrow M'_{Pb} + M^{5'}_{W} + 3V^{\cdot\cdot}_{O} + PbWO_4 \tag{3.2}$$

$$M_2O + PWO \rightarrow 2M'_{Pb} + 2Pb^{4'}_{W} + 5V^{\cdot\cdot}_{O} + 2WO_3 \tag{3.3}$$

$$M_2O + PWO \rightarrow 2M^{5'}_{W} + 5V^{\cdot\cdot}_{O} + 2WO_3 \tag{3.4}$$

The dopants we consider here include the alkali metal ions from Li^+ to K^+. We note that for every dopant ion, the original compound is, in fact, the corresponding carbonate. At temperatures above 1123 °C (the melting point of PWO), however, they first decompose into simple oxides. In all calculations, therefore, the lattice energies of oxides [30], i.e. −30.51 eV for Li_2O, −26.29 eV for Na_2O and −23.18 eV for K_2O, are incorporated to derive the solution energies.

The dependence of the calculated solution energies on the cation radius is shown in figure 1. Two main points are revealed: first, the substitution of a lead ion by alkali ions, with charge compensated by an oxygen vacancy, i.e. equation (3.1), is the most favourable reaction from the viewpoint of energy. Second, the energies of all solution reactions, from Li^+ to K^+, have a tendency to decrease, indicating the substitution solutions of large dopant ions are energetically more favourable, while the substitution mechanism no longer works for small ions, i.e. Li^+. As a matter of fact, the Li^+ ion in PWO has been found to exist in the form of an interstitial ion [31].

The possible mechanisms of pentavalent ion doping include two simple (equations (3.5) and (3.9)) and three complex (equations (3.6)–(3.8)) substitution reactions. The results are similar to that of the monovalent doping, therefore we only present here the calculated energies of Nb-doping.

$$Nb_2O_5 + PWO \rightarrow 2Nb'_{W} + V^{\cdot\cdot}_{O} + 2WO_3 \qquad \Delta E = 1.38\ \text{eV/dopant} \tag{3.5}$$

$$Nb_2O_5 + PWO \rightarrow 2Nb'_{W} + 3V''_{Pb} + 2W^{4\cdot}_{Pb} + 5PbO \qquad \Delta E = 47.66\ \text{eV/dopant} \tag{3.6}$$

$$Nb_2O_5 + PWO \rightarrow Nb'_{W} + M^{3\cdot}_{Pb} + O''_i + 2PbWO_4 \qquad \Delta E = 7.90\ \text{eV/dopant} \tag{3.7}$$

$$Nb_2O_5 + PWO \rightarrow 2Nb'_{W} + 2W^{4\cdot}_{Pb} + 3O''_i + 2PbO \qquad \Delta E = 280.6\ \text{eV/dopant} \tag{3.8}$$

$$Nb_2O_5 + PWO \rightarrow 2Nb^{3\cdot}_{Pb} + 3O''_i + 2PbO \qquad \Delta E = 19.28\ \text{eV/dopant.} \tag{3.9}$$

As can be seen from the calculated solution energies, the Nb^{5+} ion preferentially enters the W site, with the creation of an oxygen vacancy to balance the excess charge, and other reactions seem unlikely to occur because of their much higher energies. This kind of doping mechanism is easy to understand because if a Nb^{5+} ion enters the Pb lattice it will produce excessively high charge in the local structure.

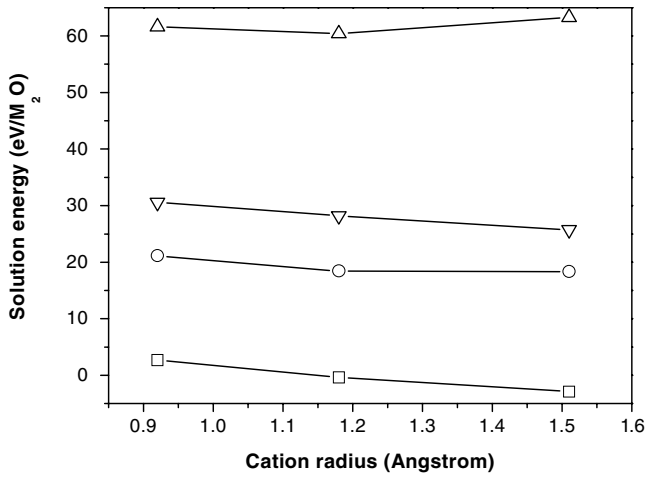

Figure 1. Dependence of the calculated solution energies of (□) equation (3.1), (○) equation (3.2), (△) equation (3.3), (▽) equation (3.4) on the monovalent cation radius.

3.2. M_2O_3 solution

In 1993, Kobayashi *et al* [32] observed that La-doping can greatly improve the PWO radiation hardness and effectively suppress the colour centre absorption bands in the short wavelength region. Since then, trivalent ions, e.g. La^{3+} [10–12], Y^{3+} [10, 12, 33], Sb^{3+} [34], Gd^{3+} [10, 13], Lu^{3+} [10, 33], Sc^{3+} [10, 33], have been the most intensively studied dopant ions in PWO. But, as mentioned above, for commonly grown crystals (doped with low concentration aliovalent ions), direct methods for determining the sites of dopant ions are impractical. The results previously reported are obtained mainly from optical experiments, the discussions on the defects of *in situ* crystals are therefore based on arguments or indirect experiments, and so they are still at the hypothesis stage.

The possible mechanisms of the trivalent ion doping reactions we have considered include three simple substitution reactions (namely equations (3.10), (3.11) and (3.14)) and two complex substitution reactions (equations (3.12) and (3.13)) as follows

$$M_2O_3 + PWO \rightarrow 2M_{Pb}^{\cdot} + V_{Pb}'' + 3PbO \tag{3.10}$$

$$M_2O_3 + PWO \rightarrow 2M_{Pb}^{\cdot} + O_i'' + 2PbO \tag{3.11}$$

$$M_2O_3 + PWO \rightarrow M_{Pb}^{\cdot} + M_W^{3'} + V_O^{\cdot\cdot} + PbWO_4 \tag{3.12}$$

$$M_2O_3 + PWO \rightarrow 2M_{Pb}^{\cdot} + 2Pb_W^{3'} + 3V_O^{\cdot\cdot} + 2WO_3 \tag{3.13}$$

$$M_2O_3 + PWO \rightarrow 2M_W^{3'} + 3V_O^{\cdot\cdot} + 2WO_3. \tag{3.14}$$

Table 3 presents the calculated reaction energies of the dopants we have considered. As can be seen, the two complex substitution reactions have relatively high solution energies, indicating they are not the energetically favourable reactions. For clarity, the dependence of the simple substitution reaction energies on the cation radius is shown in figure 2, from where sufficient information to demonstrate the doping mechanism for one specified dopant ion is exhibited.

First, for all ions considered here, the substitution reaction on the Pb lattice, with the excess positive charge compensated by a lead vacancy, has the lowest solution energy, suggesting a most favourable solution process. This conclusion is generally consistent with those previously

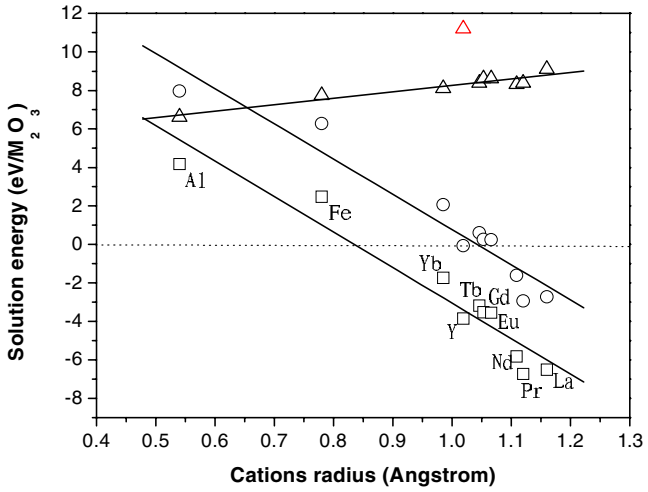

Figure 2. Dependence of the calculated solution energies of (□) equation (3.10); (○) equation (3.11); (△) equation (3.14) on the trivalent cation radius. Solid lines denote the fitted curves.

Table 3. Calculated solution energies (eV/M_2O_3) of trivalent ion doping.

			Equation				
Ions	Radius (Å)	Lattice energy (eV)	(3.10)	(3.11)	(3.12)	(3.13)	(3.14)
Al^{3+}	0.54	−157.60	4.18	7.96	7.16	24.4	6.62
Fe^{3+}	0.78	−152.34	2.48	6.68	6.87	22.7	6.87
Yb^{3+}	0.985	−137.43	−1.73	2.05	4.95	18.49	8.11
Y^{3+}	1.019	−136.39	−3.85	−0.07	5.44	16.36	11.21
Tb^{3+}	1.046	−130.82	−3.18	0.6	4.36	17.04	8.38
Gd^{3+}	1.053	−129.56	−3.52	0.26	4.31	16.7	8.62
Eu^{3+}	1.066	−129.28	−3.54	0.24	4.3	16.68	8.62
Nd^{3+}	1.109	−133.74	−5.82	−1.62	3.37	14.4	8.32
Pr^{3+}	1.12	−132.33	−6.73	−2.95	2.59	13.49	8.39
La^{3+}	1.16	−128.15	−6.51	−2.73	3.06	13.71	9.11

reported. For instance, in a La^{3+}-doped PWO crystal, Han *et al* [35] observed a classical relaxation peak when studying its dielectric properties, and considered it to be induced by the dipole movement of La^{3+} and a lead vacancy, i.e. the $[2(La_{Pb}^{3+})^{\cdot}–V''_{Pb}]$ dimers. Furthermore, this coincides with a recently reported positron annihilation experiment, which suggests that La^{3+} ion doping in PWO increases the concentration of lead vacancies [36]. We note that in a recent x-ray single diffraction of PWO doped with 1% mol La^{3+} ions, the abnormally high thermal factor at the Wyckoff 4b site also suggests the existence of lead vacancies around the Pb sublattice [37].

Second, for those ions with large radius, i.e. Nd^{3+}, Pr^{3+}, La^{3+}, a substitution reaction with the creation of an oxygen interstitial ion (namely equation (3.11)) seems to possibly occur since it has negative solution energy. In fact, the interstitial oxygen ion has been evidenced by an EXAFS experiment in very high (∼15% mol ratio) La^{3+}-doped PWO crystals [38]. We note that Y-doping, unexpectedly, has also tends to create an interstitial oxygen ion. The reason is not clear, however, interstitial oxygen ions have been evidenced in dielectric loss

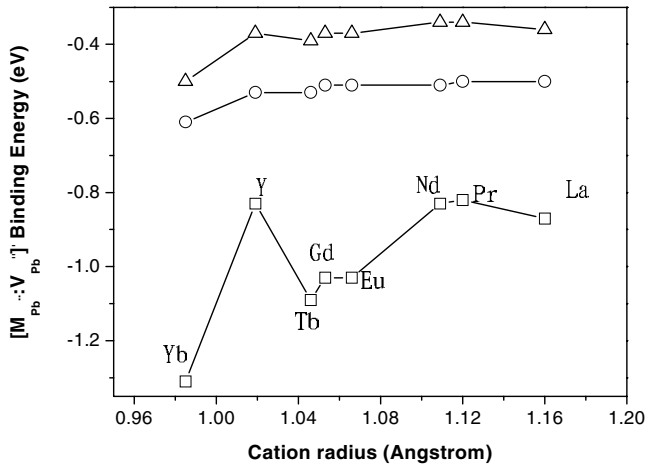

Figure 3. Binding energies of M^{3+} dopant cations to a lead vacancy, namely $[(M^{3+}_{Pb})^{\cdot}–V''_{Pb}]$, in the form of (□) nn; (○) nnn, and (△) nnnn configurations.

spectra in both La- and Y-doped PWO crystals, where they were considered to correlate with the so-called 'β-relaxation peak' [19].

Third, for small ions, e.g. Al^{3+} and Fe^{3+}, there is an increasing tendency to simple substitution on the W site (equation (3.14)) rather than on the Pb site, suggesting that small ions might preferentially enter the W lattice. Though there is no direct structural evidence, the conclusions derived from the systemically investigated absorption spectra of trivalent ions doping offer enough explanation that the small Sc^{3+} ion does not follow the doping mechanism expected for other trivalent ions, e.g. La^{3+} and Y^{3+} ions [10].

3.3. Association of extrinsic defects

Defect pairs or aggregates have been found in many materials, such as the doped Perovskite $KTaO_3$ [17] and doped superconductor YBCO [39]. They have much influence on the crystal properties. In pure PWO crystals, aggregates of the simple vacancy pair (V''_{Pb}:$V^{\cdot\cdot}_{O}$) and dimers ($2V''_{Pb}$:$V^{\cdot\cdot}_{O}$) have been evidenced in the crystal [15]. Do foreign ions form similar clusters in PWO? If yes, which configuration leads to the strongest interaction? As a matter of fact, La dimers or La small aggregates have been considered as the 'killer sites' in decay kinetics and thermoluminescence of PWO, i.e. the La^{3+} crystal, where Nikl *et al* [40] has observed two different kinds of decay processes, one of which is strongly suppressed in the case of high La concentrations. To answer these questions, in this section, we discuss the stability of extrinsic defect clusters composed of trivalent ions.

The magnitude of this interaction is related to the binding energy, $\boldsymbol{E}_b$, which is based on the calculation of cluster binding energies with respect to the constituent defects. In the case of the dimer configuration, the binding energy can be calculated as follows,

$$\boldsymbol{E}_b = \boldsymbol{E}([2(M^{3+}_{Pb})^{\cdot}–V''_{Pb}]) - 2\boldsymbol{E}([M^{3+}_{Pb}]^{\cdot})–\boldsymbol{E}([V''_{Pb}]). \tag{3.15}$$

As described in the above section, a substitution reaction with the dopant ion entering the Pb site and with the charge compensated by a lead vacancy, is the predominant reaction. Accordingly, we consider the stability of the simple pair $[(M^{3+}_{Pb})^{\cdot}–V''_{Pb}]$ and the $[2(M^{3+}_{Pb})^{\cdot}–V''_{Pb}]$ dimer configuration. The results are shown in figures 3 and 4, respectively.

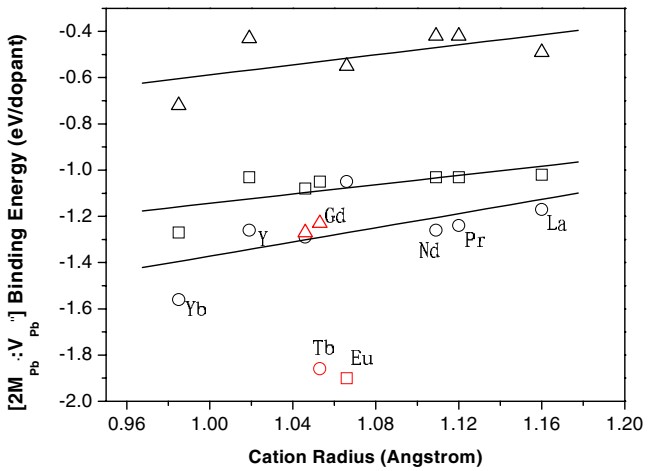

Figure 4. Binding energies of $[2(M_{Pb}^{3+})^{\cdot}–V''_{Pb}]$ clusters in the form of (□) [1st:1st]; (○) [1st:2nd]; (△) [1st:3rd] configurations. Solid lines denote the fitted curves.

From figure 3, we know that all the binding energies of the nearest neighbour (nn), the next nearest neighbour (nnn) and the next next nearest neighbour (nnnn) configurations have negative values, indicating that the dopant ions have a strong tendency to bind together. A comparison of them shows that, for all cations considered, the nn configuration is the most energetically favourable. However, for the $[2(M_{Pb}^{3+})^{\cdot}–V''_{Pb}]$ clusters, one discerns that the [1st:2nd] configuration is the most energetically favourable. The exception coincides with $[2(Eu_{Pb}^{3+})^{\cdot}–V''_{Pb}]$, where the [1st:1st] dimer configuration is found to be more stable than other configurations (figure 3). The reason for this is still not obvious, but it might relate to the interatomic potentials we have used, because, as indicated in table 1, the tendency of the lattice energy of oxides to decrease coincides with an exception around Eu_2O_3.

Another point we can conclude is that the dimer configuration, $[2(M_{Pb}^{3+})^{\cdot}–V''_{Pb}]$, is bound with relatively lower energy than the $[(M_{Pb}^{3+})^{\cdot}–V''_{Pb}]$ clusters, implying the former might be the prime cluster in the investigated crystals. This may be explained from the viewpoint of charge compensation, that is, the negatively charged $[(M_{Pb}^{3+})^{\cdot}–V''_{Pb}]$ defect is not a stable one; it should form into a neutral cluster, namely $[2(M_{Pb}^{3+})^{\cdot}–V''_{Pb}]$. We note this conclusion is consistent with reported conclusions [35].

4. Discussion

As mentioned above, aliovalent ion doping, especially trivalent ion doping, can significantly improve crystal scintillation properties [13, 29, 32]. However, almost all explanations for the doping mechanism previously reported are without exception based on arguments or indirect experiments, in other words, one always determines the lattice site that the dopant ion occupies by comparing the formal charge, electronegativity and ionic radius of the doped and the substituted ions. It is generally correct and therefore this work presents enough evidence for the conclusions previously reported and provides a sound basis for future work.

For instance, if one takes the computed results into account, one can easily understand why aliovalent doping can significantly suppress the intrinsic 350 nm absorption band. It has been documented that the intensity of the absorption band peaking around 350 nm rests with the difference number (DN) between the lead vacancy and the oxygen vacancy [16]; the bigger the DN is, the heavier the 350 nm absorption it shows. According to our simulation, both

monovalent and pentavalent ion doping will simultaneously increase the number of oxygen vacancies, and the DN, therefore, should be decreased. As a result, the crystal will show less absorption at the wavelength around 350 nm. For PWO doped with trivalent ions, we present an explanations as follows. As concluded from the above simulation results, trivalent ion doping always induces the creation of $[2(M_{Pb}^{3+})^{\cdot}-V''_{Pb}]$ clusters, which therefore bind some lead vacancies so that the number of 'active' vacancies is decreased. Accordingly, the value of DN is decreased and therefore the 350 nm absorption band is suppressed.

Based on above discussions on the relationship between trivalent ions doping and the intrinsic 350 nm absorption band, the following comments may be useful in understanding why trivalent ion doping can also significantly improve the radiation hardness of PWO. It has been well established that the intrinsic 350 nm absorption band has a linear relationship with the 420 nm radiation-induced absorption band [9]. We stress that, in the field of PWO, the radiation hardness is commonly evaluated by the intensity of the radiation-induced 420 nm absorption band. Therefore, a linear relationship between the intrinsic 350 nm absorption band and the crystal radiation hardness can be derived; the stronger the intrinsic 350 nm absorption band a crystal has, the worse radiation hardness it has. In addition, the conclusions of Auffray *et al* [41] from more than 100 full-size PWO also supports the viewpoint. They have derived that crystals with heavy intrinsic absorption around 350 nm has the worst radiation hardness, while crystals with no intrinsic 350 nm absorption show good radiation hardness. In summary, trivalent ions can significantly suppress the intrinsic 350 nm absorption band, hence inducing a $<$420 nm radiation-induced absorption band, and so the radiation hardness of the crystal, of course, is improved.

Another point of interest focuses on the creation of an interstitial oxygen ion. The creation of an interstitial oxygen ion (equation (3.11)) and lead vacancy (equation (3.10)) are competitive reactions of trivalent ion substitution. Our results clearly show that, despite the creation of a lead vacancy being the most energetically favourable, the reaction creating the interstitial oxygen ion can also possibility occur. This means that equation (3.10) should be the predominant reaction of trivalent ion doping, while equation (3.11) might take place when conditions are suitable, though we do not know here what the 'suitable conditions' are in detail. One should be cautious in giving any explanation for them due to the significant thermodynamic implications behind the negative solution energies. In general, our simulation results agree with the experimental results in [19] and [38].

In addition, our results show that the solution energy of trivalent dopants is a strong function of the dopant cation radius, which can be used to predict and explain the behaviour of those ions we have not simulated due to the lack of suitable lattice energies of oxides, e.g. Sb_2O_3. Experimental results show that the absorption spectra of Sb-doped PWO show characteristics of both trivalent and pentavalent ion doping [34]. Considering that antimony is a mid-sized ion and contains two stable valences, +3 and +5, one can easily predict that Sb ions exist in PWO in two forms: Sb^{3+}, which occupies the Pb-lattice, and Sb^{5+}, which occupies the W-lattice.

5. Conclusions

A computer simulation method has been used to study the mechanisms of substitution reactions. The present study demonstrates the importance of local structural features of aliovalent ion doped PWO, which are difficult to probe by conventional experiment techniques. Our results and discussions have drawn attention to three features as follows:

(1) The most energetically favourable solution of monovalent ion doping is when a foreign ion enters the Pb-lattice, simultaneously producing an oxygen vacancy to compensate for

the excess negative charge. Pentavalent ions, on the other hand, occupy preferentially the W sites, balanced by oxygen vacancies.

(2) Trivalent ions preferentially enter the Pb sites, with the charge compensated mainly by lead vacancies. However, in the case of large dopant ions, i.e. Nd^{3+}, Pr^{3+}, La^{3+}, the solution does not preclude the coexistence of an oxygen interstitial ion, and in the case of small ions, it may occupy the W sites.

(3) The calculated binding energies of trivalent ion doping indicate a strong tendency toward the creation of defect clusters, the $[(M_{Pb}^{3+})^{\cdot}–V''_{Pb}]$ simple pair and the $[2(M_{Pb}^{3+})^{\cdot}–V''_{Pb}]$ dimers. Moreover, the neutral $[2(M_{Pb}^{3+})^{\cdot}–V''_{Pb}]$ dimer configuration is suggested as the dominant cluster in crystal.

(4) Based on the simulated results, explanations for the relationships between the aliovalent ion doping, the suppression of colour centre absorption bands and the improvement of radiation hardness of PWO are presented.

Finally, due to the limited experimental information on the structural data of low concentration aliovalent-doped PWO, one should be cautious to give an explanation for these data. But, in general, they accord well with the conclusions based on other experimental results. Our results, therefore, in this case have clear predictive value.

Acknowledgments

We are grateful to Dr J D Gale for the GULP program. This work was financially supported by the National Science Foundation of China (Grant no 50172054) and the Science and Technology Commission of Shanghai Municipality.

References

[1] Barishevski V G, Korzhik M V, Moroz V I, Pavlenko V B, Lobko A F, Fedorov A A, Kachanov V A, Solovyanov S G, Zadneprovskii D N, Nefedov V A, Dorogovin P V and Nagornaya L L 1992 *Nucl. Instrum. Methods Phys. Res.* A **322** 231

[2] Lecoq P, Dafinei I, Auffray E, Schneegans M, Korzhik M V, Missevitch O V, Pavlenko V B, Fedorov A A, Annenkov A N, Kostylev V L and Ligun V D 1995 *Nucl. Instrum. Methods Phys. Res.* A **365** 291

[3] Zhu R Y, Ma D A, Newman H B, Woody C L, Kierstead J A, Stoll S P and Levy P W 1996 *Nucl. Instrum. Methods Phys. Res.* A **376** 319

[4] Nessi-Tedaldi F 1998 *Nucl. Instrum. Methods Phys. Res.* A **408** 266

[5] Nikl M, Niiscii K, Hybler J, Chval J and Reiche P 1996 *Phys. Status Solidi* b **196** K7

[6] Annenkov A, Auffray E, Korzhik M V, Lecoq P and Peigneux J-P 1998 *Phys. Status Solidi* a **170** 47

[7] Lin Qisheng, Feng Xiqi, Man Zhengyong, Zhang Yanxing, Yin Zhiwen and Zhang Qiren 2001 *Solid State Commun.* **118** 221

[8] Zhu R Y, Deng Q, Newman H, Woody C L, Kierstead J A and Stoll S P 1995 *IEEE Trans. Nucl. Sci.* **45** 686

[9] Han Baoguo, Feng Xiqi, Hu Guangqin, Zhang Yanxing and Yin Zhiwen 1999 *J. Appl. Phys.* **86** 3571

[10] Kobayshi M, Usuki Y, Ishii M, Senguttuvan N, Tanji K, Chiba M, Hara K, Takano H, Nikl M, Bohacek P, Baccaro S, Cecilia A and Diemoz M 1999 *Nucl. Instrum. Methods Phys. Res.* A **434** 412

[11] Kobayshi M, Usuki Y, Ishii M, Yazawa T, Hara K, Tanaka M, Nikl M, Baccaro S, Cecilia A, Diemoz M and Dafinei I 1998 *Nucl. Instrum. Methods Phys. Res.* A **404** 149

[12] Auffray E, Lecoq P, Korzhik M V, Annenkov A, Jarolimek O, Nikl M, Baccaro S, Cecilia A, Diemoz M and Dafinei I 1998 *Nucl. Instrum. Methods Phys. Res.* A **402** 75

[13] Baccaro S, Bohacek P, Borgia B, Cecilia A, Croci S, Dafinei I, Diemoz M, Fabeni P, Ishii M, Kobayshii M, Martini M, Montecchi M, Nikl M, Nitsch K, Organtini G, Pazzi G P, Usuki Y and Vedda A 1997 *Phys. Status Solidi* a **164** R9

[14] Lei Ning, Han Baoguo, Feng Xiqi, Hu Guangqin, Zhang Yanxing and Yin Zhiwen 1997 *Phys. Status Solidi* a **170** 37

[15] Lin Qisheng, Feng Xiqi and Man Zhenyong 2001 *Phys. Rev.* B **63** 134105

[16] Lin Qisheng, Feng Xiqi, Man Zhenyong, Shi Zaoshu and Zhang Qiren 2000 *Phys. Status Solidi* a **181** R1
[17] Exner M, Donnerberg H, Catlow C R A and Schirmer O F 1995 *Phys. Rev.* B **52** 3930
[18] Nikl M, Rosa J, Niiscii K, Asatryan H R, Baccaro S, Cecilia A, Montecchi M, Borgia B, Dafinei I, Diemoz M and Lecoq P 1997 *Mater. Sci. Forum* **239–241** 271
[19] Wensheng Li 2000 *PhD Thesis* Hong Kong, Baptist University
[20] Mott N F and Littlelton M J 1938 *Trans. Faraday Soc.* **34** 485
[21] Gale J D 1996 *General Utility Lattice Program* (London: Imperial College)
[22] Gale J D 1996 *Phil. Mag.* B **73** 3
[23] Catlow C R A 1989 *J. Chem. Soc. Faraday Trans. 2* **85** 335
[24] Lidiard A B 1989 *J. Chem. Soc. Faraday Trans. 2* **85** 341
[25] Born M 1923 *Atomtheorie des Festen Zustandes* (Leipzig: Teubner)
[26] Dick B J and Overhauser A W 1958 *Phys. Rev.* **112** 90
[27] Islam M S, Lazure S, Vannier R, Nowogrocki G and Mairesse G 1998 *J. Mater. Chem.* **8** 655
[28] Korzhik M V 1995 *Proc. Int. Workshop on Lead Tungstate Crystals (SCINT'95, Delft, Netherland)* p 493
[29] Annenkov A, Fedorov A A, Galez Ph, Kachano V A, Kozhik M V, Ligun V D, Moreau J M, Neffdov V N, Pavlenko V B, Peigneux J-P, Timoschenko T N and Zadneprovskii B A 1996 *Phys. Status Solidi* a **156** 493
[30] Bush T S, Gale J D, Catlow C R A and Battle P 1994 *J. Mater. Chem.* **4** 831
[31] Esaka T, Kamata M and Saito H 1996 *Solid State Ion.* **86–88** 73
[32] Kobayshi M, Ishii M, Usuki Y and Yahagi H 1993 *Nucl. Instrum. Methods Phys. Res.* A **333** 429
[33] Nikl M, Boháček P, Mihóková E, Martini M, Meinardi F, Vedda A, Fabeni P, Pazzi G P, Kobayshi M and Ishii M 2000 *J. Appl. Phys.* **87** 4243
[34] Liu Xiancai, Hu Guangqin, Feng Xiqi, Li Peijun, Zhang Mingrong, Xu Li and Yin Zhiwen 1999 *Chin. Phys. Lett.* **16** 761
[35] Han Baoguo, Feng Xiqi, Hu Guangqin, Wang Pingchu and Yin Zhiwen 1998 *J. Appl. Phys.* **84** 2831
[36] Tang Xuefeng, Gu Mu, Tong Hongyong, Liang Ling, Yao Minzheng, Cheng Linyan, liao Jinying, Shen Binfu, Qu Xiangdong, Yin Zhiwen, Xu Weixing and Wang Jingchen 2000 *Acta Phys. Sin.* **49** 2007
[37] Lin Qisheng, Feng Xiqi and Chen Jiutong 2000 *J. Alloys Compounds* **307** 245
[38] Lin Qisheng and Feng Xiqi 2001 *Jiegou Huaxue* **20** 214
[39] Islam M S and Ananthamohan C 1991 *Phys. Rev.* B **44** 9492
[40] Nikl M, Boháček P, Nitsch K, Mihóková E, Martini M, Vedda A, Croci S, Pazzi G P, Fabeni P, Baccaro S, Borgia B, Dafinei I, Diemoz M, Organtini G, Auffray E, Lecoq P, Kobayshi M, Ishii M and Usuki Y 1997 *Appl. Phys. Lett.* **71** 3755
[41] Auffray E, Dafinei I, Gautheron F, Lafond-Puyet O, Lecoq P and Schneegans M 1995 *Proc. Int. Workshop on Lead Tungstate Crystals (SCINT'95, Delft, the Netherlands)* p 282
[42] Baetzold R C 1993 *Phys. Rev.* B **48** 5789